*LAUTECH Journal of Engineering and Technology 12(2) 2018: 88-95*

# IMPROVED INTRINSIC STRESS MODELS FOR THIN FILMS BASED ON SURFACE STRESS

**Asafa T. B.**

Mechanical Engineering Department, Ladoke Akintola University of Technology, PMB 4000, Ogbomoso, Oyo State, Nigeria. e-mail: tbasafa@lautech.edu.ng

## ABSTRACT

***Study of stress evolution in thin films has been an area of rigorous research for the past few decades. In spite of these research efforts, understanding stress generation and relaxation remains incomplete. In this study, a modified surface stress based approach for modeling intrinsic stresses in thin film using dome-shaped islands and hexagonal shaped grains is proposed. Equations that describe stress evolution at the precoalescence, coalescence and postcoalescence growth stages were derived. The results of the models were then compared to some previous models and validated with experimentally obtained values for copper and silver films at various growth stages. For Cu films deposited on silicon substrates, intrinsic stresses of -200, 140 to 230 and -260 to -80 MPa were obtained for precoalescence, coalescence and steady state postcoalescence stages, respectively while the current models gave -261, 102 and -115MPa. For continuous film, the current model gave -115 MPa which is comparable to -140 MPa obtained from an experimental study conducted on Cu thin films. Furthermore, parametric studies showed that the directions of growth for both intrinsic and steady state stress are converse. Thus, the results obtained indicate that the current models are reliably and can be used for accurate stress prediction. The predictions of the current models are closer to the experimental values than any of the previous models.***

**Key words**: surface stress, intrinsic stress, dome shape, hexagonal shape

## INTRODUCTION

Thin films are currently deployed for various technological applications ranging from micro/nano-electromechanical systems (M/NEMS) like sensors and actuators to magnetic storage media, and thermal barrier coatings among others (Tesfamichaela et al., 2012). One of the critical requirements for successful application of thin films is the ability to control and reproduce the manufacturing processes. Consequently, understanding the effects of growth conditions and materials properties on the resulting residual stresses is necessary to fabricate low stress thin films (Tello and Bower, 2008; Pei at al., 2017; Xie, et al., 2017). Irrespective of fabrication method adopted, thin film-based structural layers usually exist under a state of internal stress which is often detrimental to the functionality and structural integrity of the final devices made therefrom. For example, the dynamic and reliability characteristics can be altered due to changes in structural stiffness (Guo, et al., 2012; Mehta, et al., 2004; Freund and Suresh, 2003;Xie, et al., 2019). Stresses in thin films may originate from thermal, intrinsic or extrinsic sources or a combination thereof (Pauleau, 2001; Evans and Hutchinson, 2009). The intrinsic stress depends on the film microstructure and material behavior (type I or type II) (Thompson, 2000). Type I materials (such as Cr, Fe and Ti films) are low mobility materials having only tensile stress during growth. They usually have columnar grain morphology making stress-thickness nearly constant throughout the growth duration. However, for type II materials such as Ag, Cu and Au, their high mobility leads to incremental stress as film thickened. Consequently, the stress changes from compressive to tensile and then compressive based on the slope of the stress-thickness curve.

A few mathematical models have been developed to estimate intrinsic stresses in thin films for type II materials. The two relevant models for the precoalescence stage are those of Laugier (1981) and Cammarata et al (2000). While the approach used by the former is based on the changes in the lattice constant, that of the latter relies on surface stresses using a cylindrical island. For the coalescence stage, the stress generation is based on reduction in surface energy / stress when a grain boundary is formed from neighboring islands. In this regards, Hoffman (1976) theorized that neighbouring crystallites spontaneously snap together when the gap between the adjacent islands reaches a critical value.

Because of the challenges associated with estimating critical gap, Nix and Clemens (1999) came up with two models using the surface energy-driven approach

similar to the Griffith principle of crack propagation. However, the models overestimate the induced stresses prompting Freund and Chason (2001) to use theory of contact of elastic solids with cohesion. This approach brought the predicted stress slightly closer to the experimental values. Cammarata et al. (2000) explored the concept of surface energy reduction to model islands zipping process and further extended the model to capture the steady-state stress in a growing film. It should be noted that only the models of Cammarata et al (2000) addressed the mechanisms of stress behavior during the precolescence and postcoalescence growth stage. However, all the models generally overestimate the intrinsic stresses compared to the experimental observations. Therefore, a more accurate mathematical model is necessary. This paper therefore reports refined models with higher accuracy for stress estimation.

## MODELING

### Approach, Justification and Assumptions

The modeling approach used in the current study is similar to the precoalescence stress model of Cammarata et al. (2000) but a dome shape island is envisioned as against a cylindrical island used by Cammarata. An evidence for the chosen shape is shown in the AFM image of Cu islands (Fig.1 a, b) prepared by electrodeposition of Cu on polycrystalline ruthenium (Guo and Searson, 2010). It is evident that the Cu deposition is still in the precoalescence stage since significant number of the islands are isolated. This island is then modeled as a dome (Fig. 1c). The curved surface stress of the island is assumed to be uniform along the entire curved surface since the whole surface is exposed to the influence of incoming gas flux. The area of the circular bottom disk of radius r is $A_{xy} = \pi r^2$ and that of the convex surface is $A_z = \pi r^2 + \pi h^2$. The volume of the dome is given by $V = \frac{\pi h}{6}(3r^2 + h^2)$. It is assumed that the curved surface of the island is associated with the surface stress $f_c$ and the interface between the circular bottom disk and the substrate is associated with the interface stress $f_i$. Due to these stresses, the in-plane Laplace pressure $\Delta P_r$ and out-of-plane $\Delta P_z$ are assumed to be generated along the radial and transverse directions, respectively. For an island with bottom area $A_{xy}$ and surface area $A_z$, the Laplace relation ($\Delta P = f\frac{dA}{dV}$) gives:

$$\Delta P_r = f_c\left(\frac{\partial A_z}{\partial r}\right)_h\left(\frac{\partial r}{\partial V}\right)_h + f_i\left(\frac{\partial A_{xy}}{\partial r}\right)_h\left(\frac{\partial r}{\partial V}\right)_h \quad (1)$$

$$\Delta P_z = f_c\left(\frac{\partial A_z}{\partial h}\right)_r\left(\frac{\partial h}{\partial V}\right)_r + f_i\left(\frac{\partial A_{xy}}{\partial h}\right)_r\left(\frac{\partial h}{\partial V}\right)_r \quad (2)$$

By substituting the expressions for $A_{xy}$, $A_z$ and V in Eq.(1) and Eq. (2); then:

$$\Delta P_r = 2(f_c + f_i)\frac{1}{h}, \text{ and } \Delta P_z = f_c\frac{4h}{r^2 + h^2} \quad (3)$$

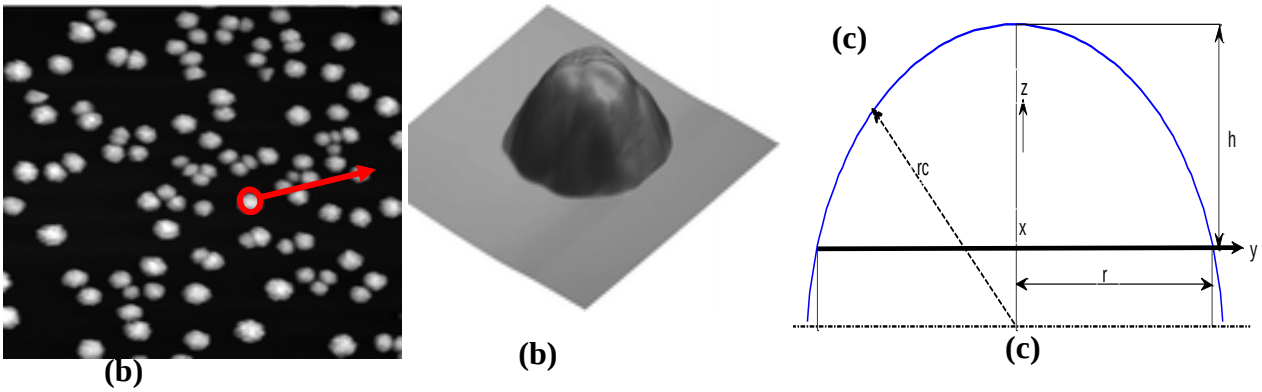


Figure 1: (a) AFM image showing significantly isolated Cu islands on oxide layer, and (b) AFM image of a single Cu island (Guo and Searson, 2010) and, (c) spherical dome shaped model of the island.

**Stress Generation at Precoalescence Stage**

Based on the island configuration of Fig. 1(c), the resulting stresses imposed on the island due to the Laplace pressure effect are $\sigma_{xx} = \sigma_{yy} = -\Delta P_r$ and $\sigma_{zz} = -\Delta P_z$. The in-plane radial strain $\varepsilon_{rr}$ induced during growth is related to the volumetric stresses by Hooke's law as $\varepsilon_{rr} = s_{11}\sigma_{xx} + s_{12}\sigma_{yy} + s_{13}\sigma_{zz}$ where $s_{11}$, $s_{12}$ and $s_{13}$ are the elastic compliances of the coordinates in the x, y and z direction, respectively. If the volumetric stress components are substituted, then the radial strain becomes:

$$\varepsilon_{rr} = -2s_{11}(f_c + f_i)\frac{1}{h} - 2s_{12}(f_c + f_i)\frac{1}{h} - 4s_{13}f_c\frac{h}{r^2 + h^2} \quad (4)$$

Following the step adopted by Cammarata et al. (2000) or CTS (i.e. Cammarata, Trimble and Srolovitz), and assuming an in-plane biaxial modulus and strain free island, the precoalescence stress can be expressed as:

$$\sigma_{pre} = 2(f_c + f_i)\left[\frac{1}{h} - \frac{1}{h_o}\right] + 2f_c(\beta - 1)\left[\frac{h}{r^2 + h^2} - \frac{h}{r_o^2 + h_o^2}\right] \quad (5)$$

Where $\beta$ depends on the crystallographic orientation and elastic compliance. The equivalent model from CTS is:

$$\sigma_{pre} = (f_c + f_i)\left(\frac{1}{h} - \frac{1}{h_o}\right) + \beta f_h\left(\frac{1}{r} - \frac{1}{r_o}\right) \quad (5.1)$$

Where $f_h$ is the surface stress due to the height of the cylindrical island.

One of the most significant differences between Eq. (5) and Eq. (5.1) is that the thickness and diameter-dependent terms are coupled and non-linear unlike in the former. This indicates that stress is non-linearly dependent on these parameters. For an elastic isotropic material where $0 < \beta < 1$, the contribution from $\beta - 1$ will be negative for Eq. (5) and just $\beta$ for Eq. (5.1). This is bound to change the sign or magnitude of the estimated stress thereby generating a new trend.

**Coalescence and Postcoalescence Stresses**

The mechanism of stress generation during island coalescence is similar to the concept discussed in Cammarata et al., 2000). The grain boundary is formed by gradual zipping of the islands as it is energetically favourable. In such a case, surface stress $f_{gb}$ associated with the grain boundary is formed. In the current case, it is assumed that the dome shaped islands coalesce to form a regular hexagonal grain of a side length $r'$, height $h'$, grain boundary area $A_{gb} = 6r'h'$, surface area $A'_{xy} = \frac{3\sqrt{3}}{2}r'^2$ and total volume $V' = \frac{3\sqrt{3}}{2}r'^2h'$ (Fig. 2a). Assuming in-plane isotropy, Laplace pressure–surface stress relation gives:

$$\Delta P'_x = (f_c + f_i)\left(\frac{\partial A'_{xy}}{\partial r'}\right)_{h'}\left(\frac{\partial r'}{\partial V'}\right)_{h'} + \frac{f_{gb}}{2}\left(\frac{\partial A_{gb}}{\partial r'}\right)_{h'}\left(\frac{\partial r'}{\partial V'}\right)_{h'} = \Delta P'_y \quad (6)$$

$$\Delta P'_z = (f_c + f_i)\left(\frac{\partial A'_{xy}}{\partial h'}\right)_{r'}\left(\frac{\partial h'}{\partial V'}\right)_{r'} + \frac{f_{gb}}{2}\left(\frac{\partial A_{gb}}{\partial h'}\right)_{r'}\left(\frac{\partial h'}{\partial V'}\right)_{r'} \quad (7)$$

Substituting for $A'_{xy}$, $A'_z$, $A_{gb}$ and $V'$, Eq. (6) and Eq. (7) become: $\Delta P'_x = \Delta P'_y = (f_c + f_i)\frac{1}{h'} + \frac{f_{gb}}{\sqrt{3}}\frac{1}{r'}$, and

$$\Delta P'_z = \frac{2f_{gb}}{\sqrt{3}}\frac{1}{r'} \quad (8)$$

The associated bi-axial strain associated with the Laplace pressure change is given by:

$$\varepsilon'_{xx} = -\frac{1}{Y}\left[\left(f_c + f_i\right)\frac{1}{h'} + \frac{f_{gb}}{\sqrt{3}}\frac{1}{r'}\right] - 2s_{13}\frac{f_{gb}}{\sqrt{3}}\frac{1}{r'} = \varepsilon'_{yy} \tag{9}$$

The extra stress $\Delta\sigma_{,cont}$ imposed by the substrate constraint on the grain as it grows from complete coalescence stage $(h'_{imp}, r'_{imp})$ to a steady state $(h', r')$ is given by:

$$\Delta\sigma_{,cont} = \left(f_c + f_i\right)\left[\frac{1}{h'} - \frac{1}{h'_{imp}}\right] + \frac{f_{gb}}{\sqrt{3}}\left[\frac{1}{r'} - \frac{1}{r'_{imp}}\right] + \frac{f_{gb}}{\sqrt{3}}\left(\beta - 1\right)\left[\frac{1}{r'} - \frac{1}{r'_{imp}}\right] \tag{10}$$

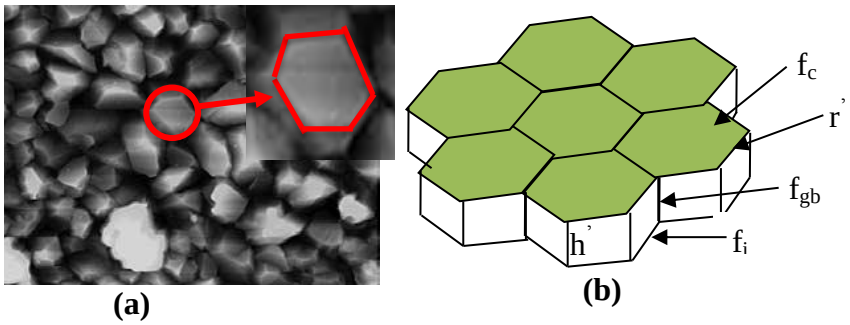


Figure 2: (a) SEM image showing grain structure in Cu film (inset is a single hexagonal grain) (Ji, 2004). Note that the grain boundaries have been etched (b) the equivalent hexagonal grain model

Since coalescence is not an instantaneous process, the change in the strain due to the grain boundary formation is evaluated at the beginning and completion of coalescence process. The induced stress $\Delta\sigma_{,imp}$ is given as:

$$\Delta\sigma_{,imp} = \left(f_c + f_i\right)\left[\frac{1}{h'_{imp}} - \frac{2}{h_{imp}}\right] + \left(\beta - 1\right)\left[\frac{f_{gb}}{\sqrt{3}}\frac{1}{r'_{imp}} - 2f_c\frac{h_{imp}}{r_{imp}^2 + h_{imp}^2}\right] + \frac{f_{gb}}{\sqrt{3}}\frac{1}{r'_{imp}} \tag{11}$$

Therefore, the total intrinsic stress for a continuous film $\sigma_{,cont}$ is the summation of Eq. (5), Eq. (10) and Eq. (11).

$$\sigma_{,cont} = \left(f_c + f_i\right)\left[\frac{1}{h'} - \frac{2}{h_o}\right] + \left(\beta - 1\right)\left[\frac{f_{gb}}{\sqrt{3}}\frac{1}{r'} - 2f_c\frac{h_o}{r_o^2 + h_o^2}\right] + \frac{f_{gb}}{\sqrt{3}}\frac{1}{r'} \tag{12}$$

The stress at coalescence can be obtained from Eq. (12) when $(h', r') = (h'_{imp}, r'_{imp})$ and the actual stress induced by the coalescence process is given by Eq. (11). For comparison, the equivalent stress model from Cammarata et al (2000) is given by:

$$\sigma = \left(f_c + f_i\right)\left(\frac{1}{h} - \frac{1}{h_o}\right) + \beta\left(\frac{f_{gb}}{2r} - \frac{f_h}{r_o}\right) \tag{12.1}$$

## RESULTS AND DISCUSSION

### Parametric studies

Equations 5, 10 and 12 were coded on MATLAB platform to explore the stress behaviour at precoalescence, coalescence and postcoalescence growth stages based on available data obtained from Cu film deposited on silicon oxide. Figure 3 (a) shows the influence of island height on the precoalescence stress using Eq. (5) and Eq. (5.1). While both CTS and the current models showed a decreasing compressive stress with increased island height, the current model indicates a smaller compressive stress similar to experimental data (Seel, 2002). For the coalescence process, the induced stress depends on both the island radius prior to impingement as well as the thickness changes over which the coalescence process takes place (Eq. 11). According to Fig. 3(b), the stress due to coalescence decreases with increased thickness at impingement and increases with island diameter at impingement for film thickness less than 4 nm. Beyond thickness of 4 nm, the stress increases with increased diameter at impingement. For instance the coalescence stress at thickness of 2 nm is 160, 60 and 40 MPa at impingement diameter of 5, 10 and 15 nm,

respectively. The slope of the stress-thickness curve is higher for smaller island at impingement compared to bigger islands as can been observed.

By computing stress over a few thickness prior to impingement, the maximum stress generated during island coalescence decreases with island size (Fig. 3c). This may account for higher compressive stress observed in the films with large grains compared to those of small grains. Also, the intrinsic stress becomes compressive during postcoalescence evolution due to increased film thickness or grain size (Fig. 3 d).

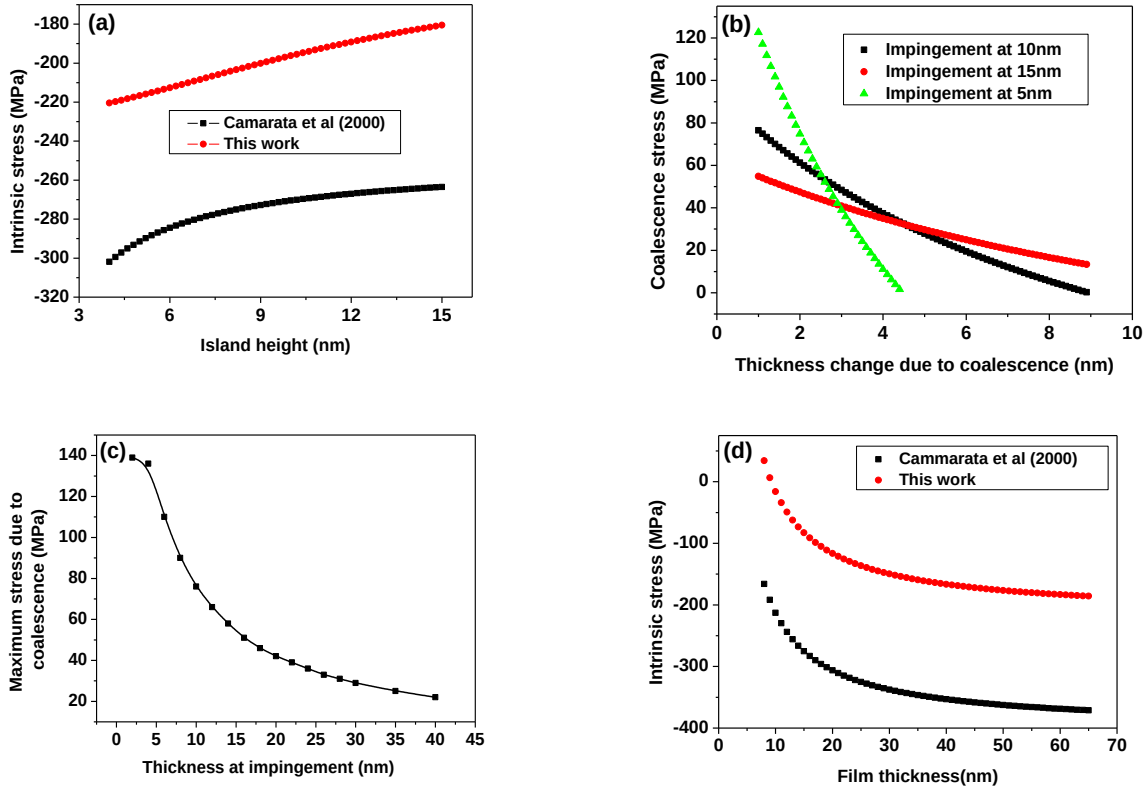


Figure 3: (a) Precoalescence stress evolution (b) stress changes due to coalescence as a function of thickness and diameter at impingement (c) maximum stress variation with thickness at impingement (d) Postcoalescence stress evolution, f = g = 0.5N/m, h= 1.5N/m, do = 2.5 nm.

**Model Comparison**

The current models are validated with experimental results from literature, and then compared to a few published models. For the precoalescence stage, the models were compared with stress evolution in thin Ag films deposited by CVD (Freund and Suresh, 2003). For silver, with $\nu = 0.37$ (Freund and Chason, 2001), the values of the surface stresses were assumed to be $f_c = f_i = f_f = 0.5N/m$ and $f_h = 1N/m$ since the surface stresses for most alkaline metals are in the range of 0.2 and 1 N/m (Cammarata et al., 2000). For a critical or lock down parameter of $h_o$ = 1.5 nm and an impingement parameter of $h_{imp}$ = 5 nm, and d = 2.5*h for silver islands just before impingement, Eq. (5) and Eq. (5.1) gave ~-42 MPa and ~ -119 MPa, respectively. This implies that the result of the current model (~-42 MPa) is closer to the experimental values ( -20 to +20 MPa) obtained from Seel (Seel, 2002) than the CTS model (-119 MPa). Also for Cu, a good agreement between experimental results (-200 MPa) and the current model (-213 MPa) was obtained (Table 1). For the choice of 2.5 as a multiplier for island diameter d, the diameters and heights of a series of silicon germanium islands were measured, and it was found that the diameter/height ratio stabilized at ~2.5 prior to coalescence. Since silicon germanium films are polycrystalline as evident from the XRD spectra published elsewhere (Asafa et al., 2013) and behave like type II materials at elevated temperature, it is expected that the island diameter/height ratio will be similar to those of Cu and Ag films.

Table 1: Predicted and measured compressive stress (MPa) prior to coalescence for Ag and Cu films

| Material/ Substrate | Fitting Parameters | Eq. (5.1) | Eq. (5) | Experiment |
|---|---|---|---|---|
| Ag/CVD oxide layer | $\nu = 0.37$ $f_c = f_i = f_f = 0.5$, $f_h = 1$ N/m[b], $h_o = 1.5$ nm, $d_o = 2.5 * h_o$nm, himp = 5 nm, $d = 2.5 * h$ nm, $\beta$ = -0.504 | -128.6 | -42 | -20 to +20[a] |
| Cu(001)/oxidized silicon | $\nu = 0.34$ $f_c = f_i = f_f = 1$, $f_h = 1.5$ N/m[b] $h_o = 2$ nm, $d_o = 2.5 * h_o$ nm, h = 5 nm, $d = 2.5 * h$ nm, $\beta$ = -0.448 | -382 | -213 | -200[a] |

[a] [Ref (Seel, 2002) [b] [Ref. (Cammarata et al., 2000)]

The postcoalescence stress models are validated with three experimental results (Seel, 2002; Abermann and Koch, 1985; Shull, 1996)). For Cu; the grain boundary energy $\gamma_{gb} = 0.715 J/m^2$, free surface energy $\gamma_s = 1.3135 J/m^2$ (Murr, 1975), elastic modulus E = 127 GPa and $\nu = 0.34$. Also $h_o = 2.5nm$, $d_o = 2.5 * h_o$ and $f_{gb} - 2f_c = -6 N/m$ were selected similar to that of Cammarata et al (2000), other parameters are similar to those in Table 1. Two important points are examined: (i) at the completion of coalescence and (ii) during a continuous or steady-state growth. Upon complete coalescence; $h_{imp} = 13nm$ and $d_{imp} = 2.5 * 13nm$ and h = 60 nm at steady stress state (Seel, 2002). The results for the post-coalescence stress models are presented in Table 2. The predictions of the current models are closer to the experimental values than any of the previous models. Both Nix-Clemens models over-exaggerate the induced stress. Freud-Chason and Seel models are slightly close to the experimental values. The coalescence and postcoalescence models of Cammarata et al. indicate compressive stresses for both stages while the experiments indicate a tensile stress for the stress just after coalescence. These results indicate that the dome shaped island is more realistic than other shape.

At the precoalescence stage, the stresses predicted by the current model are slightly more compressive than those of the experiments (see Table 2). One of the possible reasons for the deviation may be due to the assumed shape of the growing islands which may not be a perfect dome. Also, the slightly lower tensile stress obtained from the experiment for the steady-state stress may be attributed to an incomplete island coalescence. In addition, the accurate determination of the interfacial stress associated with the grain boundary $f_{gb}$ might require an extensive experimental investigation. However, since $f_c - f_{gb}/2 > 0$ is a necessary condition for a grain boundary to form, the assumption of $f_{gb} - 2f_c$ = -6 N/m may as well be justified. Finally, it is assumed that the surface, interfacial and grain boundary stress/energy are dependent on the material and not the growth conditions. This may require further investigation.

On a general note, the current approaches do not include other mechanisms of stress generation and relaxation which have been the focus of previous studies (Freund and Chason, 2001; Abermann and Koch, 1985)]. It may be necessary to investigate a hybrid approach where the surface stress method is combined with any of the atomic-level models. While the current models are simple, they may also provide a useful framework for stress evolution study in thin films.

Table 2: Stresses at coalescence and continuous stages for Cu (001) films

| S/N | Model/ Experiment | Source (s) | Stress after complete coalescence (MPa) | Stress in the continuous film (MPa) |
|---|---|---|---|---|
| 1 | Nix-Clemens 1 | Nix and Clemens, 1999 | 5320 | 2476 |
| 2 | Nix-Clemens 2 | Nix and Clemens, 1999 | 6158 | 2866 |
| 3 | Freund-Chason | Freund and Chason, 2001 | 616 | 222 |
| 4 | Seel et al | Seel at al, 2000) | 1532 | 713 |
| 5 | Cammarata et al. | Eq. (12.1) | -150 | -346 |
| 6 | This work | Eq. (12) | 102 | -115 |
| 7 | Experiment 1 | Seel, 2002 | 175 | -107±33 |
| 8 | Experiment 2 | Abermann and Koch, 1985 | 230 | -80 |
| 9 | Experiment 3 | Shull, 1996 | 140 | -260±25 |

## CONCLUSIONS

It has been shown that surface stress can explain the intrinsic stress observed during film growth. The current model is based on the assumption of dome shaped islands for the precoalescence state. These isolated islands induce stress when their lattice parameters are constrained in response to the volumetric expansion. An assumption of hexagonal grains is made for the postcoalescence state. By balancing the forces due to the Laplace pressure and those of the surface stresses, models that account for the precoalescence compressive stress, the coalescence tensile stress and the postcoalescence compressive stress observed in Cu and Ag thin films were derived. It was observed that island/grain shape changes can account for the type of stress obtained during thin film deposition. The results of the current models are in better agreement with experimental observations compared to those of other published models.

## REFERENCES

Abermann, R., and Koch, R. (1985). The internal stress in thin silver, copper and gold films, , 129, (1–2)71-78

Asafa, T. B., Bryce, G., Severi, S., Said, S., and Witvrouw, A. (2013). Multi-response Optimization of Ultrathin Poly-SiGe Films Characteristics for Nano- Electromechanical Systems (NEMS) Using the Grey-Taguchi Technique. Microelect Eng. *111*, 229–233.

Cammarata, R. C., Trimble, T. M., and Srolovitz, D. (2000). Surface stress model for intrinsic stresses in thin films. *J. Mater. Res., 15,11*, 2468 - 2474.

Evans, A., and Hutchinson, J. (2009). A critical assessment of theories of strain gradient plasticity. *Acta Materialia, 57*, 1675-1688.

Freund, L. B., and Chason, E. (2001). Model for stress generated upon contact of neighboring islands on the surface of a substrate . *J. Appl. Phys. 89*, 4866 - 4873 .

Freund, L., & Suresh, S. (2003). *Thin Film Materials: Stress, Defects Formation and Surface Evolution.* Cambridge: Cambridge University Press.

Guo, B. W., Wen, L., Helin, P., Claes, G., De Coster, J., Du Bois, B., Witvrouw, A. (2012). Poly-SiGe-Based MEMS Thin-Film Encapsulation. *Journal of Microelectromechanical Systems , 21 91),* 110 - 120 .

Guo, L., and Searson, P. C. (2010). Influence of anion on the kinetics of copper island growth. 2(11):2431-5.

Hoffman, R. (1976). Stresses in thin films: the relevance of grain boundaries and impurities. *Thin Solid Films, 34* , 185.

Ji, Y., Zhong, T., Li, Z. Wang, X., Luo, D., Xia, Y., Liu, Z. (2004). Grain structure and crystallographic orientation in Cu damascene lines, Microele Engineering, 71, 2, 182-189

Laugier, M. ( 1981). Intrinsic stress in thin films of vacuum evaporated LiF and ZnS using an improved cantilevered plate technique . *Vacuum,31, 3*, 155-157 .

Mehta, A., Gromova, M., Rusu, C., Baert, K., van Hoof, C., & Witvrouw, A. (2004). Novel high growth rate processes for depositing poly-SiGestructural layers at CMOS compatible temperatures. *Proceedings of the MEMS*, (pp. 721-724). Maastricht, Netherland.

Murr, L. (1975). *Interfacial Phenomena in Metals and Alloys.* Reading, M.A.: Addison-Wesley.

Nix, W., and Clemens, M. (1999). Crystallite coalescence: A mechanism for intrinsic tensile stresses in thin films. *J. Mater. Res., 14, 8*, 3467 - 3473.

Pauleau, Y. (2001). Generation and evolution of residual stresses in physical vapour-deposited thin film. *Vacuum 61*, 175 - 181.

Pei, F., Buchovecky, E., Bower, A., and Chason, E. (2017). Stress evolution and whisker growth during thermal cycling of Sn films: A comparison of analytical modeling and experiments. *Acta Materialia, 129*, 462-473.

Seel, S. C, Thompsona, C., Hearne, S., and Floro, J. (2000). Tensile stress evolution during deposition of Volmer–Weber thin films. *Journal of Applied Physics, 88, 12* , 7079.

Seel, S. (2002). *Modified N-C.* Ph.D. Thesis, Massachusset Institute of Technology.

Shull, A. (1996). *Measurement of stress during deposition of copper and silverthin films and multilayers.* Cambridge, M.A.: Havard University.

Tello, J., & Bower, A. (2008). Numerical simulations of stress generation and evolution in Volmer–Weber thin films. *Journal of the Mechanics and Physics of Solids 56*, 2727–2747.

Tesfamichaela, T., Ponzoni, A., Ahsana, M., & Faglia, G. (2012). Gas sensing characteristics of Fe-doped tungsten oxide thin films. *http://dx.doi.org/10.1016/j.snb.2012.04.032*.

Xie, H., Zhang, Q., Song, H., Shi, B., & Kang, Y. (2017). Modeling and in situ characterization of lithiation-induced stress in electrodes during the coupled mechano-electro-chemical process. *Journal of Power Sources, 342* , 896-903.

Wagner, L. K., & Grossman, J. C. (2008). Light-Induced Defects in Amorphous Silicon Solar Cells. *Physical Review Letters 101*, 265501.

Xie, H., Song, H., Jian-gang, G., Kang, Y., and Zhang, Q. (2019). In situ measurement of rate-dependent strain/stress evolution and mechanism exploration in graphene electrodes during electrochemical process. *Carbon, 144*, 342-350.